nomethylpiperidine (AMP) solution, 0.4 M: 0.5 g of AMP are dissolved in 10 mL of THF and stored at 4 °C for at least 1 h before use. Inside a cold room, amine-SBA-15 (1.0 g) is placed in a 15 mL peptide synthesis vessel and 10 mL of the CC solution is added. The mixture is incubated while shaking for 24 h at 4 °C . Then, the solution is removed by filtration and the solid is rinsed with 30 mL portions of methanol, dichloromethane, and THF. The AMP solution (10 mL) is added to the amine–SBA-15 and incubated again for 24 h at 4 °C while shaking. Afterward, the silica is washed as previously described and dried under vacuum. The same procedure is repeated to increase the generation (size) of the dendrimers attached to the SBA-15.

Powder X-ray diffraction (XRD) was performed on a Bruker-AXS D8 powder diffractometer using Cu Kα radiation over a range of 0.8 to 10° 2$\theta$. Transmission electron microscopy was performed on a JEOL 2010 microscope with a lanthanum hexaboride filament and an excitation voltage of 200 kV. TGA data were collected on a TG 209C Iris from Netzsch Instruments over a temperature range of 25 to 600 °C using oxygen as a carrier gas and a temperature ramping rate of 10 °C min$^{-1}$. Mass spectra were aquired using MALDI-MS on an Applied Biosystems Voyager-DE STR Biospectrometry Workstation. Matrix-assisted laser desorption/ionization time-of-flight (MALDI-TOF) spectra were recorded in linear ion mode with an Applied Biosystems Voyager DE-STR mass spectrometer (ABI, Framingham, MA). Positive ions were generated by using a nitrogen laser pulse ($y$ = 337 nm, 20 Hz) and accelerated under 20 kV using delayed extraction (550 ns) before entering the time-of-flight mass spectrometer. Laser strength was adjusted to provide minimal fragmentation and optimal signal-to-noise ratio. An average of 200 laser shots was used for each spectrum, and data were processed with the accompanying Voyager software package. The sample was prepared using the overlayer method [18,19] with 2,4,6-trihydroxyacetophenone (THAP) as has been described previously [20]. The sample cocktail, approximately 1 μM dendrimer and 10 mg mL$^{-1}$ THAP solution in methanol, was spotted in 1 μL aliquots on top of a 100 mg mL$^{-1}$ THAP matrix bed. Attenuated total reflection Fourier-transform infrared (ATR-FTIR) measurements were performed on a Perkin–Elmer Spectrum One FT-IR spectrometer. Nitrogen adsorption experiments were performed on a Micromeritics ASAP 2010 micropore system. Approximately 0.1 g of sample was degassed under vacuum at room temperature for 4 h, then at 60 °C for 4 h, then at 100 °C for 20 h before analysis. The mesopore size distribution was calculated from the adsorption branch of the isotherm using the Barret–Joyner–Halenda (BJH) method with a modified equation for the statistical film thickness [21,22].

Received: October 20, 2003
Final version: February 2, 2004

[1] A. P. Wight, M. E. Davis, *Chem. Rev.* **2002**, *102*, 3589.
[2] K. Moller, T. Bein, *Chem. Mater.* **1998**, *10*, 2950.
[3] C. E. Fowler, S. L. Burkett, S. Mann, *Chem. Commun.* **1997**, 1769.
[4] N. K. Raman, M. T. Anderson, C. J. Brinker, *Chem. Mater.* **1996**, *8*, 16821.
[5] M. H. Lim, A. Stein, *Chem. Mater.* **1999**, *11*, 3285.
[6] M. F. Ottaviani, N. J. Turro, S. Jockbush, D. A. Tomalia, *J. Phys. Chem. B* **2003**, *107*, 2046.
[7] I. Diaz, B. Garcia, B. Alsonso, C. M. Casado, M. Moran, J. Losada, J. Perez-Pariente, *Chem. Mater.* **2003**, *15*, 1073.
[8] A. S. H. King, L. J. Twyman, *J. Chem. Soc., Perkins Trans. 1* **2002**, 2209.
[9] K. Sakai, T. C. Teng, A. Katada, T. Harada, K. Yoshida, K. Yamanaka, Y. Asami, M. Sakata, C. Hirayama, M. Kunitake, *Chem. Mater.* **2003**, *15*, 4091.
[10] J. P. K. Reynhardt, H. Alper, *J. Org. Chem.* **2003**, *68*, 8353.
[11] M. W. McKittrick, C. W. Jones, *Chem. Mater.* **2003**, *15*, 1132.
[12] W. Zhang, E. E. Simanek, *Org. Lett.* **2000**, *2*, 843.
[13] W. Zhang, D. T. I. Nowlan, L. M. Thomson, W. M. Lackowski, E. E. Simanek, *J. Am. Chem. Soc.* **2001**, *123*, 8914.
[14] W. Zhang, S. E. Tichey, L. M. Perez, G. Maria, P. A. Lindahl, E. E. Simanek, *J. Am. Chem. Soc.* **2003**, *125*, 5086.
[15] E. J. Acosta, Y. J. Deng, G. N. White, J. B. Dixon, K. J. McInnes, S. A. Senseman, A. S. Frantzen, E. E. Simanek, *Chem. Mater.* **2003**, *15*, 2903.
[16] F. Rouquerol, J. Roquerol, K. Sing, *Adsorption by Powders and Porous Solids*, Academic, San Diego, CA **1999**.
[17] D. Y. Zhao, Q. S. Huo, J. L. Feng, B. F. Chmelka, G. D. Stucky, *J. Am. Chem. Soc.* **1998**, *120*, 6024.
[18] O. Vorm, P. Roepstorff, M. Mann, *Anal. Chem.* **1994**, *66*, 3281.
[19] J. M. Koomen, W. K. Russell, J. M. Hettick, D. H. Russell, *Anal. Chem.* **2000**, *72*, 3860.
[20] L. Zhou, D. R. Russell, M. Zhao, R. M. Crooks, *Macromolecules* **2001**, *34*, 3567–3573.
[21] E. P. Barrett, L. G. Joyner, P. P. Halenda, *J. Am. Chem. Soc.* **1951**, *73*, 373.
[22] M. Kruk, M. Jaroniec, A. Sayari, *Langmuir* **1997**, *13*, 6267.

# Low-Temperature, Surface-Mediated Foaming of Polymer Films**

By *Srinivas Siripurapu*, *Joseph M. DeSimone*, *Saad A. Khan*, and *Richard J. Spontak**

Polymer foams show tremendous promise over their dense analogs in terms of material, cost, weight, and waste reduction, as well as property enhancement, multiple functionality, and post-use recyclability. Here, we show for the first time that ultraporous polymer films, which are of growing interest in technologies such as molecular separations, microelectronics, biotechnology, and pharmaceuticals, can be controllably produced with high-pressure $CO_2$ by physically constraining a film between external hard surfaces during foaming. Vastly improved cell densities and homogeneity reflect a substantive reduction in the rate of $CO_2$ diffusion upon depressurization. We extend this *reverse-barrier* strategy to include internal surfaces by dispersing non-porous silica nanoparticles (hard sur-

[*] Prof. R. J. Spontak, Dr. S. Siripurapu, Prof. J. M. DeSimone, Prof. S. A. Khan
Department of Chemical Engineering
North Carolina State University
Raleigh, NC 27695 (USA)
E-mail: rich_spontak@ncsu.edu
Prof. R. J. Spontak
Department of Materials Science & Engineering
North Carolina State University
Raleigh, NC 27695 (USA)
Prof. J. M. DeSimone
Department of Chemistry, University of North Carolina
Chapel Hill, NC 27599 (USA)

[**] This study was supported by the Kenan Center for the Utilization of Carbon Dioxide in Manufacturing and the STC Program of the National Science Foundation under Agreement No. CHE-9876674. We gratefully thank Dr. I. Manners (University of Toronto) for the PFS, and Mr. D. J. Frankowski (North Carolina State University) for the preliminary results of foamed PFS.


DOI: 10.1002/adma.200306068
© 2004 WILEY-VCH Verlag GmbH & Co. KGaA, Weinheim

ADVANCED MATERIALS

faces) or $CO_2$-philic polymer surfactants (soft surfaces) in the polymer matrix. An overall increase in cell density is particularly pronounced at low foaming temperatures, which require less energy consumption. Our findings further reveal that the surfactants permit polymer foaming at low pressures where $CO_2$ exists as a liquid.

Highly porous materials have attracted broad interest as supports for smart membranes,[1–3] fuel cells,[4] reflective displays,[5] and sensors.[6] Depending on the size scale and regularity of the pore size and position, such materials may also serve as optical devices[7,8] and templates.[9] The benefits of using polymeric materials directly in such emergent technologies include low cost and weight, versatility, mechanical robustness, and facile processability. Thermoplastic polymers, produced at an annual volume of approximately thirty million kilograms in the US alone,[10] are ideally suited for diverse technologies wherein dimensional stability, mechanical rigidity, and recyclability constitute important design factors. Porous foams derived from various thermoplastic polymers augment many of the above benefits by reducing bulk density and, hence, the amount of requisite material, as well as the corresponding cost and weight.[11,12] Moreover, foams account for less material waste and energy expenditure incurred during processing and after disposal, both of which constitute important considerations from an environmental standpoint. In several instances, polymer foams exhibit superior mechanical properties, such as increased impact strength and stiffness-to-weight ratio, relative to their dense counterparts[13] and, for this reason, are used in building and automotive construction. Similarly, polymer foams commonly serve as insulation and packaging media.

Foaming polymers in a batch or continuous process generally requires physical dissolution of an inert gas or vapor (the "blowing agent") in a molten polymer to form a homogeneous solution, which is subsequently subjected to a rapid pressure quench to generate a supersaturated solution. Bubble nucleation within the polymer matrix ensues according to the mechanism embodied in classical nucleation theory (CNT)[14] and is responsible for the development of cells that grow until the temperature of the polymer is sufficiently reduced to lock-in the cell morphology. For amorphous (glassy) thermoplastics, the temperature at which this occurs is the glass transition temperature ($T_g$). While many blowing agents are commercially used to produce porous media, one that has attracted widespread interest is high-pressure $CO_2$,[15] since it is readily available, inexpensive, and environmentally benign. Another desirable attribute of $CO_2$ is that it is not combustible, unlike some of the organic compounds currently used for this purpose. Moreover, $CO_2$ exhibits tunable liquid-like solubility but gas-like viscosity under supercritical fluid conditions,[16] which can be readily accessed due to its relatively low critical point at $T_c = 31.1\,^{\circ}C$ and $P_c = 72.8$ atm. It is well known that the physical properties of polymers are strongly influenced by exposure to $CO_2$,[17,18] and several independent studies[12–15,19–23] have demonstrated that microcellular polymer foams with cell densities exceeding $10^9$ cells $cm^{-3}$ can be generated by subjecting bulk polymers to high-pressure $CO_2$.

While most endeavors to foam polymers have traditionally focused on bulk systems, there is considerable and growing interest in controllably producing porous polymer films for use in the separations and microelectronics industries. Similarly, such films have attracted attention as drug-release vehicles, catalyst supports, and tissue scaffolds, depending on cell size and connectivity (open versus closed cell morphology). Efforts specifically designed to yield nanoporous polymer films with a low dielectric constant ($k$) conventionally rely on several multistage strategies,[24] such as the self-organization of block copolymers. Selective removal of the dispersed component through chemical, radiation, or thermal treatment renders an ultraporous polymer film.[25] Using temperature-induced phase separation, recent studies[26] confirm that low-$k$ nanoporous polymers ($k = 1.77$) can be generated in polyimides by high-temperature single-step foaming with $CO_2$ as the physical blowing agent. Attempts to prepare, in systematic fashion, polymer films possessing ultraporous morphologies are, however, often thwarted by cell coalescence that occurs as growing cells impinge upon each other and cell walls rupture during depressurization.

The depressurization step in foaming occurs primarily by rapid diffusion of the blowing agent from the film surface, since the area afforded by the film edges is negligible in comparison. This scenario is illustrated in Figure 1a, which shows a schematic diagram of the conventional depressurization process and a scanning electron microscopy (SEM) image of a corresponding poly(methyl methacrylate) (PMMA) film foamed with $CO_2$ at 340 atm and 40 °C. Large cells measuring on the order of 10 μm in diameter are evident in this image. To reduce the extent to which individual cells coalesce during depressurization and thereby retain an ultraporous polymer

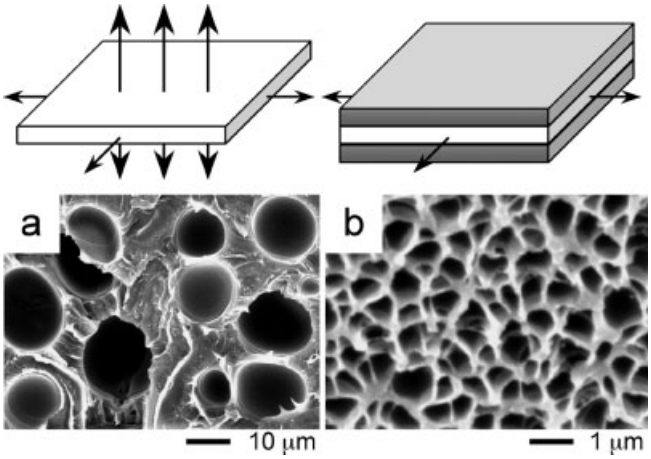


**Figure 1.** SEM images of PMMA films foamed a) without and b) with surface confinement, schematically depicted in the accompanying illustrations, in supercritical $CO_2$ at 40 °C and 340 atm. The foamed films have been cross-fractured in liquid nitrogen, pulse-coated with ~25 nm of Au/Pd, and imaged on a Philips 505T scanning electron microscope (FEI Co., Hillsboro, OR) operated at an accelerating voltage of 10–12 kV.

 © 2004 WILEY-VCH Verlag GmbH & Co. KGaA, Weinheim 

film, we propose an innovative, yet simple, strategy in which a physical, $CO_2$-impermeable surface barrier is used to slow the rate at which $CO_2$ diffuses from the film. In this reverse-barrier configuration, $CO_2$ can only escape from the film edges, which is expected to increase the residence time of $CO_2$ in the film, and eliminate property and morphology gradients along the surface normal. We further explore the benefit of surface-mediated foaming through the addition of *hard* (rigid and impermeable) siliceous nanoparticles or *soft* (flexible and permeable) polymer surfactants to the polymer matrix. These additives not only hinder the diffusion of $CO_2$ escaping from the polymer matrix, but also endow the polymer with a large population of internal surfaces for the concurrent heterogeneous nucleation of $CO_2$ bubbles.

Figure 1b shows the same PMMA film used in Figure 1a after surface-mediated foaming (depicted in the accompanying illustration). The dramatic reduction in cell size (to $<1\ \mu m$) and corresponding increase in cell density (to $\sim 5\times10^{11}$ cells cm$^{-3}$) are immediately evident upon comparing the two images. While *micro*porous foams with cells measuring on the order of 100–300 nm can be routinely achieved with the current films, efforts employing thinner films have resulted in cell sizes less than 100 nm (*nano*porous foams). Another feature of interest in foams is the cell shape. In Figure 1a, the large cells remain circular in cross-section after coalescence of smaller cells. This shape is consistent with the lowest surface-to-volume ratio attainable for a dispersion. Close examination of the foam morphology displayed in Figure 1b reveals that the cells appear polyhedral, indicating that the cell walls undergo extensional deformation, but not much rupture, as the cells grow during hindered $CO_2$ removal from the confined film. In a comparably foamed amorphous poly(ferrocenylsilane) (PFS), the cells orient along the surface normal due to non-negligible surface roughness of the film and, hence, incomplete contact between the confining steel plates and the polymer film. This result reveals that subtle variation in the surface (versus edge) diffusion of $CO_2$ in surface-mediated polymer foaming can likewise be used to template anisotropic foams. The effects of $CO_2$ pressure under isothermal conditions (40 °C) and temperature under isobaric conditions (340 atm) on cell density ($N$) in PMMA are presented in Figure 2 and confirm that $N$ is maximized at low foaming temperature, which is contrary to contemporary design strategies based on retrograde vitrification,[25] and high $CO_2$ pressure. Low temperatures (near the $T_g$ of the $CO_2$-plasticized polymer solution) expedite polymer vitrification and, consequently, solidification of a desired foam morphology at the low-energy-consumption conditions required to ensure commercial viability and resource accountability. High $CO_2$ pressures provide a large supply of $CO_2$ molecules, which can subsequently form a large population of cell nuclei upon depressurization. On the basis of this systematic comparison, all further studies will be performed at relatively low temperature (40 °C) and high pressure (170–340 atm).

The curves included in Figure 2 correspond to predictions from an extended version of CNT[16] that we developed to account for PMMA/$CO_2$ interfacial tension ($\gamma$). Generally speaking, the rate of homogeneous nucleation of cells per unit volume ($N_h$) can be written as[20]

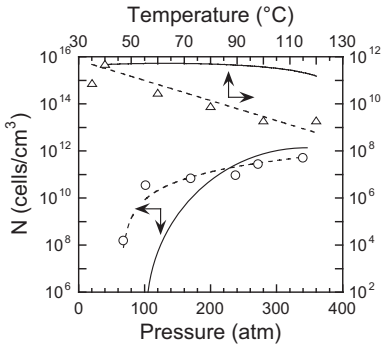


**Figure 2.** Cell densities ($N$) of PMMA films subjected to surface-mediated foaming in $CO_2$ under conditions of constant temperature (40 °C, O) or constant pressure (340 atm, △). The solid lines denote predictions from the CNT, whereas the dashed lines identify predictions from our modified CNT described in the text, in which the interfacial tension is determined from

$$\gamma = \frac{2^{1/2}}{\nu_1}\left[\kappa_{11}^{1/2} + \kappa_{22}^{1/2}\left(\Delta\rho_2/\Delta\rho_1\right)\right]\int_{\phi_1^{I}}^{\phi_1^{II}} \tilde{\rho}\,\Delta a^{1/2}\,d\phi_1$$

Here, $\Delta\rho_i$ is the density difference of component $i$ ($i=1$ for $CO_2$ and $i=2$ for PMMA) partitioned between two coexisting phases (I and II), $\tilde{\rho}$ is the reduced density from an equation of state, $\phi_i$ is the volume fraction of species $i$, $\kappa_{ii}$ is the self-interaction parameter for species $i$, $\nu_1$ is the solvent unit volume, and $\Delta a$ is the difference between the actual interfacial free energy density and that which would exist if each phase was separated by a line of zero thickness [27]. Experimental cell densities are computed from SEM images according to the procedure proposed by Kumar and Suh [19].

$$N_h = Cf\ \exp\left(-\frac{\Delta G_h}{k_B T}\right) \tag{1}$$

where $C$ is the concentration of $CO_2$ molecules in the polymer solution, $k_B$ is the Boltzmann constant and $T$ denotes absolute temperature. The energy barrier for homogeneous nucleation ($\Delta G_h$) is related to $\gamma$ by[20]

$$\Delta G_h = \frac{16\pi\gamma^3}{3\Delta P^2} \tag{2}$$

where $\Delta P$ represents the magnitude of the pressure quench during depressurization. The collision frequency of $CO_2$ molecules ($f$) is determined from $4\pi r_c^3 Z R_{imp}$, where $Z$ is the Zeldovich factor accounting for cell coalescence, $R_{imp}$ is the rate of impingement of gas molecules per unit area, and $r_c$ is the critical nucleus radius ($=2\gamma/\Delta P$). Unlike CNT, $\gamma$ is explicitly calculated here from the Sanchez–Lacombe equation of state developed for compressible polymer systems.[27] The theoretical cell density is ascertained from

$$N = \int_{P_{sat}}^{P_{atm}} \frac{N_h}{(dP/dt)}\,dP \tag{3}$$

where $P_{sat}$ is the saturation pressure of $CO_2$, $P_{atm}$ is atmospheric pressure and $dP/dt$ identifies the depressurization rate.

 © 2004 WILEY-VCH Verlag GmbH & Co. KGaA, Weinheim 

ADVANCED MATERIALS

The favorable agreement between experimental and predicted cell densities in Figure 2 confirms that this classical theoretical framework not only embodies the underlying physical mechanism of pore cell development in the present surface-mediated foams, but also yields quantitative predictions for $N(T,P)$ when $\gamma$ is accurately described.

To ascertain if the surface-mediated foaming concept can be further improved through the addition of internal surfaces that hinder $CO_2$ diffusion by creating a more tortuous diffusive pathway and simultaneously induce heterogeneous nucleation, PMMA films containing different concentrations of nanosilica particles have been exposed to high-pressure $CO_2$. Representative nanocomposite foams generated at 40 °C and 170 atm with 0 to 8 wt.-% nanosilica are displayed in Figures 3a–c and reveal that the nanosilica amplifies the effect of the external surface confinement imposed. While the mean cell diameter of the foam is insensitive to nanosilica content,

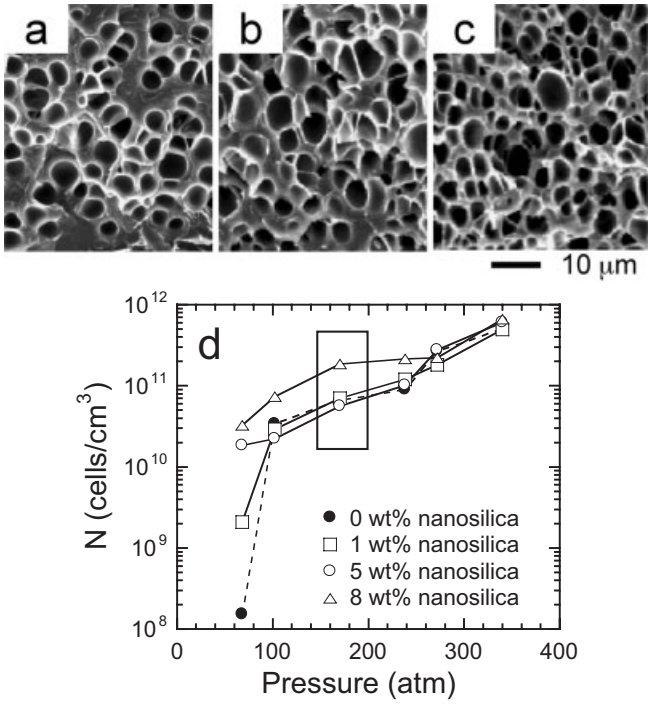


**Figure 3.** SEM images of surface-confined PMMA films containing different concentrations of nanosilica (in wt.-%)—a) 0, b) 5, and c) 8—and foamed in supercritical $CO_2$ at 40 °C and 170 atm. The dependence of cell density on foaming pressure is provided in (d) for four nanosilica concentrations (see the legend). Cell densities extracted from images such as those displayed in (a–c) are identified by the rectangle.

the cell density increases noticeably. Values of $N$ extracted from images such as these are presented as functions of nanosilica concentration and $CO_2$ pressure at 40 °C in Figure 3d, and clearly demonstrate that $N$ increases systematically with increasing nanosilica concentration up to 8 wt.-%—abruptly at low pressures, but more modestly at high pressures. This observed trend reflects the relative importance of heterogeneous nucleation, which dominates over homogeneous nucleation in the event that the amount of $CO_2$ available for bubble nucleation is limited (at low $CO_2$ pressures). At higher pressures, both mechanisms appear to be of comparable significance. If the nanosilica concentration is increased further to 12 wt.-%, the cell density is found to decrease markedly due to nanoparticle aggregation, as confirmed by transmission electron microscopy, and less effective surface area is available for heterogeneous nucleation of $CO_2$.

Addition of 0.5–2.0 wt.-% graft or diblock copolymer surfactant to the PMMA prior to film casting results in the formation of dispersed micelles with $CO_2$-philic cores, which serve as nanoscale reservoirs for $CO_2$ during foaming. The surface-mediated foam morphologies of these blends are strikingly similar to those of the nanocomposites at 40 °C and high $CO_2$ pressures (under supercritical conditions), in which case we now turn our attention to low pressures. Under these conditions, the influence of the polymer surfactants is profound, as evidenced by the SEM images displayed in Figure 4. This series clearly shows that, at *liquid* $CO_2$ conditions (30 °C and 61.2 atm), the neat PMMA films (Fig. 4a) do not foam even with surface confinement. Addition of up to 8 wt.-%

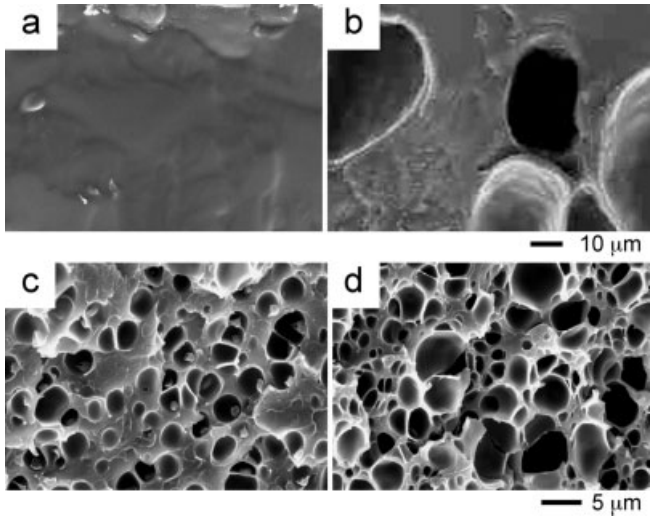


**Figure 4.** SEM images of surface-confined PMMA films containing different additives—a) no additive, b) 8 wt.-% nanosilica, c) 2 wt.-% PMMA-*g*-PDMS graft copolymer synthesized by macromonomer free radical polymerization and d) 2 wt.-% PMMA-*b*-PFOMA diblock copolymer synthesized by ATRP—and foamed in liquid $CO_2$ at 30 °C and 61.2 atm.

nanosilica (Fig. 4b) promotes limited nucleation with small cells coalescing into a few large ones. In marked contrast, incorporation of 2 wt.-% graft or diblock copolymer (Figs. 4c,d, respectively) yields a remarkably well-defined microcellular foam morphology with cell diameters measuring on the order of 1–5 μm.

We have shown that surface-mediated foaming of polymer films is a general strategy that can be used as a physical means by which to control foam morphology—cell size, shape, connectivity, and orientation—in amorphous polymer thin films,

 © 2004 WILEY-VCH Verlag GmbH & Co. KGaA, Weinheim 

especially at low foaming temperatures. In this work, we have likewise demonstrated that this approach is entirely compatible with, but not limited to, $CO_2$ as a physical blowing agent. The fundamental premise underlying this methodology is that smaller and more numerous cells can be retained in the final foam by limiting the mass transfer rate of the blowing agent during depressurization. We have used solid, impermeable plates for this purpose, but the concept readily extends to various mold geometries and laminate structures insofar as the residence time of the blowing agent in the polymer solution is kept less than the time required for bubble coalescence. An unforeseen benefit of our reverse-barrier approach to foaming polymer films, which further differentiates it from foaming based solely on temperature-induced phase separation,[26] is that the dense (non-porous) skin layer located at both polymer/plate surfaces is surprisingly thin (about one cell diameter thick), if existent at all. Reduction of this layer not only reduces the dielectric constant and dissipation factor of the polymer, but also permits closer examination of surface bubbles, as well as the response of polymer thin films to a compressible fluid.[28] In some cases of foamed PFS, no dense surface layer is discernible, and the oriented cells extend completely through the thin film.

Physical addition of hard nanoparticles or soft surfactants to the polymer matrix results in the formation of internal surfaces that further serve to hinder gas diffusion while promoting concurrent heterogeneous nucleation, the results of which are more pronounced at low pressures and temperatures. Such operating conditions are of crucial commercial consideration since they require minimal energy consumption and capital investment. While ongoing efforts have focused on discontinuous or multistage methods to harness ultraporous polymer films,[22,24,25] we have demonstrated that single-step foaming of polymer thin films can be greatly enhanced in a straightforward and general manner through physical confinement, and can likewise be used to generate ultraporous films by regulating the fundamental mechanism by which foaming occurs. Systematic variation of the confinement and environmental parameters explored here can be used to control cell size, shape, connectivity, and orientation in thin polymer foams that are to be used as-is or, alternatively, as functional precursors to other ultraporous media,[15] such as metallated ceramics[29] in the case of PFS.

## *Experimental*

Atactic PMMA ($M_n = 70$ kg mol$^{-1}$, $M_w = 107$ kg mol$^{-1}$) was provided by Elf Atochem N.A. (King of Prussia, PA) and purified prior to use. Nanosilica possessing a hydroxyl-terminated surface and a mean particle diameter of 10–12 nm was obtained from Nissan Chemicals (Houston, TX). A poly(dimethylsiloxane) (PDMS) macromonomer ($M_n = 10$ kg mol$^{-1}$) with a monomethacrylate end group, methyl methacrylate (MMA) monomer, and 1,1-dihydroperfluorooctyl methacrylate (FOMA) monomer, used in the surfactant synthesis, were supplied by Aldrich Chemicals (St. Louis, MO). Carbon dioxide (> 99.8 % pure) was obtained from National Specialty Gases (Durham, NC), and reagent-grade toluene (99.98 % pure) was purchased from Aldrich Chemicals and used as-received. The synthesis of PDMS-based graft copolymers employed a macromonomer technique wherein the graft copolymer was prepared by free-radical copolymerization of the PDMS macromonomer with de-inhibited MMA in the presence of 2,2-asobisisobutyronitrile (AIBN) as initiator. The mean graft ratio of the resultant copolymer was discerned from $^1$H NMR to be ~ 0.5. According to gel permeation chromatography (GPC) analysis, $M_n$ of the PMMA backbone was 40 kg mol$^{-1}$. An asymmetric diblock copolymer composed of PMMA and poly(1,1-dihydroperfluorooctyl methacrylate) (PFOMA) was synthesized by atom transfer radical polymerization (ATRP) [30]. The copolymer was produced via formation of a PMMA macroinitiator and subsequent addition of FOMA monomer. The number-average molecular weights of the PMMA and PFOMA blocks were determined from $^1$H NMR and GPC to be 30 and 3 kg mol$^{-1}$, respectively.

Films measuring 50 to 100 μm thick, as discerned by profilometry, were prepared by casting concentrated PMMA/toluene solutions with and without additives (nanoparticles or copolymers) on glass plates. Cast films were dried for 48 h at ambient temperature and then placed under vacuum at 40 °C for another 24 h. Densified PMMA films were removed from the glass plate, and the free-standing films were subjected to further vacuum drying at 40 °C for an additional 12 h, and then cut into 1.3 cm × 2.5 cm rectangles. Specimens containing nanosilica or copolymer were microtomed and examined by transmission electron microscopy (TEM) to ensure uniform dispersion. Each film was then tightly sandwiched between two smooth stainless steel plates in a homemade foaming die. The die was inserted into a high-pressure view chamber, which is designed to achieve uniform heating (±0.5 °C) and connected to an ISCO high-pressure pump. The conditions within the chamber, as well as the depressurization rate, were computer-controlled. Upon attaining a desired foaming temperature, each specimen was saturated with $CO_2$ for 6 h at pressures ranging from 61.2 to 340 atm. After this time, the chamber was depressurized at a constant rate of ~ 68 atm s$^{-1}$ under isothermal conditions and then quiescently cooled to yield the final foam.

Received: August 26, 2003
Final version: February 19, 2004
Published online: June 3, 2004

[1] Y. Ito, Y. Ochiai, Y. S. Park, Y. Imanishi, *J. Am. Chem. Soc.* **1997**, *119*, 1619.
[2] T. C. Merkel, B. D. Freeman, R. J. Spontak, Z. He, I. Pinnau, P. Meakin, A. J. Hill, *Science* **2002**, *296*, 519.
[3] Y. Iwasaki, S. Uchiyama, K. Kurita, N. Morimoto, N. Nakabayashi, *Biomaterials* **2002**, *23*, 3421.
[4] F. Q. Liu, B. Yi, D. Xing, J. Yu, H. Zhang, *J. Membr. Sci.* **2003**, *212*, 213.
[5] K. Robbie, D. J. Broer, M. J. Brett, *Nature* **1999**, *399*, 764.
[6] V. S. Y. Lin, K. Motesharei, K. S. Dancil, M. J. Sailor, M. R. Ghadiri, *Science* **1997**, *278*, 840.
[7] S. Walheim, E. Schaffer, J. Mlynek, U. Steiner, *Science* **1999**, *283*, 520.
[8] M. Srinivasarao, D. Collings, A. Philips, S. Patel, *Science* **2001**, *292*, 79.
[9] P. Jiang, J. F. Bertone, V. L. Colvin, *Science* **2001**, *291*, 453.
[10] W. J. Storck, M. McCoy, M. S. Reisch, H. Tullo, M. Heylin, P. L. Short, A. M. Thayer, J.-F. Tremblay, *Chem. Eng. News* **2002**, *80*, 42.
[11] *Polymeric Foams: Science and Technology* (Eds: V. Kumar, J. E. Weller), American Chemical Society, Washington, DC **1997**.
[12] S. Siripurapu, Y. J. Gay, J. R. Royer, J. M. DeSimone, R. J. Spontak, S. A. Khan, *Polymer* **2002**, *43*, 5511.
[13] D. F. Baldwin, C. B. Park, N. P. Suh, *Polym. Eng. Sci.* **1996**, *36*, 1425.
[14] J. S. Colton, N. P. Suh, *Polym. Eng. Sci.* **1987**, *27*, 500.
[15] A. I. Cooper, *Adv. Mater.* **2003**, *15*, 1049.
[16] J. M. DeSimone, *Science* **2002**, *297*, 799.

 © 2004 WILEY-VCH Verlag GmbH & Co. KGaA, Weinheim 

ADVANCED MATERIALS

[17] L. J. Gerhardt, C. W. Manke, E. J. Gulari, *J. Polym. Sci. B: Polym. Phys.* **1997**, *35*, 523.
[18] J. R. Royer, J. M. DeSimone, S. A. Khan, *J. Polym. Sci. B: Polym. Phys.* **2001**, *39*, 3055.
[19] V. Kumar, N. P. Suh, *Polym. Eng. Sci*. **1990**, *30*, 1323.
[20] S. K. Goel, E. J. Beckman, *Polym. Eng. Sci*. **1994**, *34*, 1137.
[21] C. M. Stafford, T. P. Russell, T. J. McCarthy, *Macromolecules* **1999**, *32*, 7610.
[22] Y. P. Handa, Z. Zhang, *J. Polym. Sci. B: Polym. Phys.* **2000**, *38*, 716.
[23] B. Krause, R. Mettinkhof, N. F. A. van der Vegt, M. Wessling, *Macromolecules* **2001**, *34*, 874.
[24] J. L. Hedrick, R. D. Miller, C. J. Hawker, K. R. Carter, W. Volksen, D. Y. Yoon, M. Trollsås, *Adv. Mater*. **1998**, *10*, 1049.
[25] T. Xu, H. C. Kim, J. DeRouchey, C. Seney, C. Levesque, P. Martin, C. M. Stafford, T. P. Russell, *Polymer* **2001**, *42*, 9091.
[26] B. Krause, G.-H. Koops, N. F. A. van der Vegt, M. Wessling, M. Wübbenhorst, J. van Turnhout, *Adv. Mater.* **2002**, *14*, 1041.
[27] K. L. Harrison, K. P. Johnston, I. C. Sanchez, *Langmuir* **1996**, *12*, 2637.
[28] T. Koga, Y. S. Seo, X. Hu, K. Shin, Y. Zhang, M. H. Rafailovich, J. C. Sokolov, B. Chu, S. K. Satija, *Europhys. Lett.* **2002**, *60*, 559.
[29] M. J. MacLachlan, M. Ginzburg, N. Coombs, T. W. Coyle, N. P. Raju, J. E. Greedan, G. A. Ozin, I. Manners, *Science* **2000**, *287*, 1460.
[30] K. Matyjaszewski, J. Xia, *Chem. Rev.* **2001**, *101*, 2921.

# Mercury(II) *N,N′*-Methyl-Phenylethyl-Dithiocarbamate and Its Use as a Precursor for the Room-Temperature Solution Deposition of β-HgS Thin Films

By *Mark Green*,* *Paul Prince*, *Martin Gardener*, and *Jonathan Steed*

Mercury chalcogenides have attracted numerous studies of late, due to the interesting properties of both thin films and nanosized materials.[1–3] Thin films of HgS are reportedly semimetals (zero-gap semiconductors — although there is still controversy regarding the band structure of such systems), whilst size effects in quantum dots such as HgE (E = S, Te) result in a widening of the bandgap, giving tuneable band-edge emission ranging the visible to the infrared regions of the electromagnetic spectrum. For example, 5 nm diameter HgTe particles emit at ca. 1500 nm, an important wavelength in telecommunications.[4]

Mercury sulphide exists in two polymorphs; α-HgS (trigonal, cinnabar) and β-HgS (zinc blende, metacinnabar). α-HgS is the stable phase, transforming to β-HgS at temperatures above 300 °C, reverting to the cinnabar phase upon cooling. Recent studies based on Shubnikov–de Haas effects in β-HgS suggest a bandgap of –0.19 eV,[5] whilst relativistic all-electron full-potential calculations suggest an inverted band structure with a small indirect energy gap of 0.05 eV due to spin–orbit coupling.[6] The unusual band structures and negative effective electron mass may mean β-HgS has potential spintronic applications.

Thin films of metal chalcogenides can be made by numerous vapor deposition and chemical bath methods; however, these have the disadvantages of a) the use of toxic precursors, such as metal alkyls and similar chalcogen sources, and b) can often give mixed-phase products.[7,8]

An attractive alternative is the use of single-source precursors, complexes where the metal–chalcogen bond is already in place and a simple decomposition mechanism results in the deposition of the semiconducting material. Single-source precursors are usually cheaper, safer, and more stable than the dual-precursor systems. There are few reports on single-source precursors for mercury chalcogenides. Crouch et al. recently reported imino-bis(diisopropyl phosphine)chalcogenide complexes of mercury as effective single-source precursors for HgE (E = S, Se) powders.[9] Steigerwald and co-workers have reported single-source routes to HgTe nanomaterials, however, the growth of the particles was fast and uncontrolled, an observation recently reproduced in the binary growth of HgTe dots.[10,11]

O'Brien has pioneered the theromolytic use of metal dithiocarbamates as single-source precursors for thin films and nanomaterials, making in-depth studies on the effects of side groups on deposition temperatures and decomposition mechanisms.[12] A very common structure for most metal(II) dithiocarbamates is simple dimeric. However, mercury dithiocarbamates, $Hg(S_2CNR_2)_2$, exist in up to five structural 'motifs' — common dimeric, distorted monomer, square planar monomer, the rarer tetramer, and the distorted dimeric eight-membered ring—the actual structure adopted is dependant of the organic functionality.[13–15] This is important when considering decomposition mechanisms, as structure and specific reactions such as the elimination of stable leaving groups are intimately related. To date, mercury dithiocarbamates have not been used as precursors for electronic materials.

In this paper, we report the synthesis of a new mercury(II) dithiocarbamate with a distorted eight-membered ring structure, mercury(II) *N,N′*-methyl-phenylethyl-dithiocarbamate, $[Hg(S_2CNMe(EtPh))_2]_2$ and its use in the facile preparation of β-HgS films. The single-crystal X-ray structure is shown in Figure 1. This route to β-HgS is highly unusual as it proceeds at room temperature in solution, yielding the usually inaccessible β-HgS phase (previous single-source routes to HgS yielded the expected α-HgS phase[9] whilst a mixed α and β

[*] Dr. M. Green,[+] Dr. P. Prince, Dr. M. Gardener
Oxonica Ltd
Begbroke Science and Business Park
Sandy Lane, Yarnton, Oxfordshire OX5 1PF (UK)
Dr. J. Steed[++]
Department of Chemistry, Kings College London
The Strand, London WC2R 2 LS (UK)
[+] Present address: Department of Physics, Kings College London, The Strand, WC2R 2LS, UK.
E-mail: mark.green@kcl.ac.uk
[++] Present address: Department of Chemistry, University of Durham, University Science Laboratories, South Road, Durham, DH1 3 LE, UK.

 © 2004 WILEY-VCH Verlag GmbH & Co. KGaA, Weinheim DOI: 10.1002/adma.200306407 